Eurographics/ IEEE-VGTC Symposium on Visualization 2010
G. Melançon, T. Munzner, and D. Weiskopf
(Guest Editors)

Volume 29 (2010), Number 3

An Evaluation of Glyph Perception for Real Symmetric Traceless Tensor Properties

T.J. Jankun-Kelly, Y.S. Lanka, and J.E. Swan II

Mississippi State University

Abstract

A perceptual study of four tensor glyphs for symmetric, real, traceless tensors was performed. Each glyph encodes three properties of the system: Orientation, uniaxiality (alignment along the direction of orientation), and biaxiality (alignment along a vector orthogonal to the orientation). Thirty users over two studies were asked to identify these three properties for each glyph type under a variety of permutations in order to evaluate the effectiveness of visually communicating the properties; response time was also measured. We discuss the significant differences found between the methods as guidance to the use of these glyphs for traceless tensor visualization.

Categories and Subject Descriptors (according to ACM CCS): I.3.3 [Computer Graphics]: Picture/Image Generation— I.3.5 [Computer Graphics]: Computational Geometry and Object Modeling—Curve, surface, solid, and object representations

1. Introduction

Tensor visualization seeks to describe volumetric or other high-dimensional properties of a system. One approach for depicting tensors is the use of glyphs: 3D shapes that act as icons encoding different parameters of the tensor [All89, AWB01, BH04, JKM06, KWH00, KW99, Kin04, SEHW02, SPL*06, SKH95, ZLK04]. An important issue in glyph visualization is the comprehensibility of such markers—how accurately do they communicate tensor characteristics? Ebert and others have investigated superquadric glyphs for general high dimension visualization [ERS*00, SEK*98]; but that study leaves open the question of the effectiveness of established tensor glyphs. In this work, we report the results of an empirical study to address that question, using nematic liquid crystal alignment tensors as basis.

As a case study, nematic liquid crystal (NLC) alignment visualization exhibits interesting properties. First, the NLC tensor is symmetric, real, and traceless, possessing different properties than the more common non-traceless tensors seen in DT-MRI visualization [ZLK04]. However, both NLC and DT-MRI visualization utilize the tensor's eigenvalues to construct their shapes, so lessons from one are applicable to the other. Second, NLC systems have clear physical parameters (orientation, alignment strength, and strength of symmetry) that need to be communicated. Finally, the existing glyphs for NLC tensors span the range of common shapes—boxes, cylinders, ellipsoids, and superquadrics. To the best of our knowledge, a study comparing the efficacy of these four canonical glyphs has not been performed.

2. Nematic Liquid Crystal Alignment

To understand NLC tensor glyphs, some background in NLC physics is required. Nematic liquid crystals are an intermediary state of matter between solid and liquid states wherein molecules have no long range positional order but exhibit local orientation alignment [Col02]. NLCs are often composed of molecular chains that posses rotational symmetry. Each individual NLC molecule can be said to orient along the molecule's axis of rotational symmetry. Depending on the environmental conditions and the nature of the NLC medium, groups of these molecules tend to align their rotational axes in different configurations (Figure 1). It is the type and strength of these macro-molecular orientations which are of interest to liquid crystal physicists.

Mathematically, the physics of the alignment of an NLC medium is represented by a second-order, real symmetric traceless tensor known as the alignment tensor $\mathbf{Q}$ [dG74, MN04]. This tensor encapsulates the director $\mathbf{n}$ (the average orientation of the molecules), the strength of the alignment

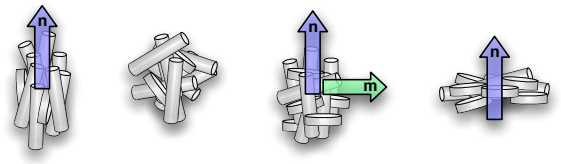

Figure 1: *The four major configuration of a nematic liquid crystal system. From left to right: Positive Uniaxial, Isotropic, Biaxial, Negative Uniaxial.*

S along $\mathbf{n}$, any secondary axis due to reflective symmetry $\mathbf{m}$ and the strength of the reflective symmetry (the *biaxiality* b). In the eigenframe, assuming $\mathbf{n} = \hat{\mathbf{x}}$ and $\mathbf{m} = \hat{\mathbf{y}}$, the alignment tensor is represented as:

$$[\mathbf{Q}]_\varepsilon = \begin{bmatrix} \frac{2}{3}S & & \\ & -\frac{1}{3}S - b_s & \\ & & -\frac{1}{3}S + b_s \end{bmatrix} = \begin{bmatrix} \lambda_1 & & \\ & \lambda_2 & \\ & & \lambda_3 \end{bmatrix} \tag{1}$$

where $b_s = \operatorname{sgn}(S)b$ and $\lambda_i \in \left[-\frac{1}{3}, \frac{2}{3}\right], |\lambda_1| \geq |\lambda_2| \geq |\lambda_3|$ are the eigenvalues. The scalar order parameter ranges from $S = 1$ when all the molecules are aligned with $\mathbf{n}$ (Figure 1, left), through zero at isotropy (Figure 1, left-middle), to $-\frac{1}{2}$ when the system is fully negative uniaxial (Figure 1, right). Similarly, the largest (in terms of absolute value) eigenvalue λ_1 is positive when S is positive, zero when isotropic, and negative otherwise. The tensor is in fact traceless so that $\mathbf{Q} = \mathbf{0}$ when the system is isotropic [dG74]. The biaxial strength b ranges from $\left[0, \frac{1}{3}|S|\right]$ with a maximum value of $\frac{1}{6}$. Of note is the relationship between the biaxiality and the sign of S—when the system is such that $\lambda_1 = -\lambda_2$ (and thus b is maximum), the sign of S (and thus the system) is undefined. Essentially, in this *neutral biaxial* state (Figure 1, right-middle), there is equal alignment with the director and the second symmetry axis. NLC tensor glyphs must thus allow distinction between these four states and gradations between them; these four states also are the extreme four states any real symmetric traceless tensor can take.

2.1. NLC Tensor Visualization

Excluding position, an NLC tensor glyph must encode three pieces of information: the director (orientation) $\mathbf{n}$, the scalar order parameter (uniaxial alignment strength) S, and the amount of biaxiality b. Instead of using these parameters directly, tensor visualization methods have used the eigensystem values. Table 1 summarizes how several NLC glyphs are constructed; Figure 2 depicts exemplar glyphs for different orientations, uniaxial strength, and biaxial strength.

Each of the four glyph types uses a different base shape; these shapes emphasize different aspects of the NLC system.

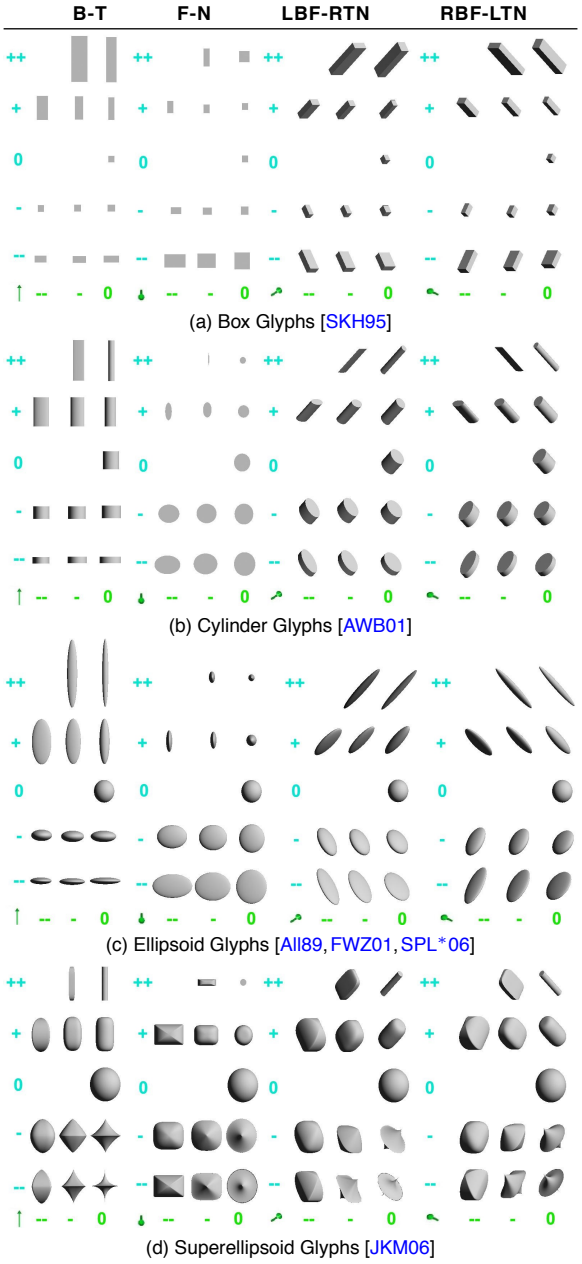

Figure 2: *Glyph types used in the study with given unaxiality (vertical axis), biaxiality (horizontal axis), and orientation levels (horizontal groups). Gaps represent invalid tensor values. See Section 3.2 for their construction.*

The box-shaped glyphs, described by Sonnet et al. [SKH95], highlight the amount of biaxiality in a system—biaxiality increases the amount of reflective (non-rotational) symmetry in the system, a feature prominent in rectangular shapes. Cylindrical glyphs [AWB01] are naturally rotation-

GLYPH	SCALING FACTORS	NOTES
Box [SKH95]	$\max(s_{\min}, \frac{1}{2}(\lambda_i + \sqrt{\frac{2}{3}\sum_i \lambda_i^2}))$	s_{min} is the minimum glyph size.
Cylinder [AWB01]	$\frac{1}{2}(\lambda_i + 0.53)$	
Ellipsoid [All89,FWZ01,SPL*06]	$\max\left(s_{\min}, \lambda_i + \frac{1}{3}\right)$	
Superellipsoid [JKM06]	$\lambda_1 \geq 0 \Rightarrow \begin{cases} s_x = s_{\max} \\ s_y = s_{\min} + (s_{\max} - s_{\min})(1 + 3\lambda_3) \\ s_z = s_{\min} + (s_{\max} - s_{\min})\left(1 - \frac{3}{2}\lambda_1\right) \end{cases}$ $\lambda_1 < 0 \Rightarrow \begin{cases} s_x = s_{\max} \\ s_y = s_{\max} \\ s_z = s_{\min} + (s_{\max} - s_{\min})\left(1 - \frac{1}{2}\lvert 3\lambda_1 + 6\lambda_3 \rvert\right) \end{cases}$	$s_{\max}$ is the maximum glyphs size. The superellipsoid shape parameters [Bar81] are: $\lambda_1 \geq 0 \Rightarrow \begin{cases} \alpha = 1 - \lvert 3\lambda_1 + 6\lambda_3 \rvert \\ \beta = 1 + 3\lambda_3 \end{cases}$ $\lambda_1 < 0 \Rightarrow \begin{cases} \alpha = 1 - \lvert 3\lambda_1 + 6\lambda_3 \rvert \\ \beta = 1 + 18\lambda_3 \end{cases}$

Table 1: *Studied NLC glyph construction based upon the references cited. Scaling factors assume* $\mathbf{n} = \hat{\mathbf{x}}, \mathbf{m} = \hat{\mathbf{y}}$.

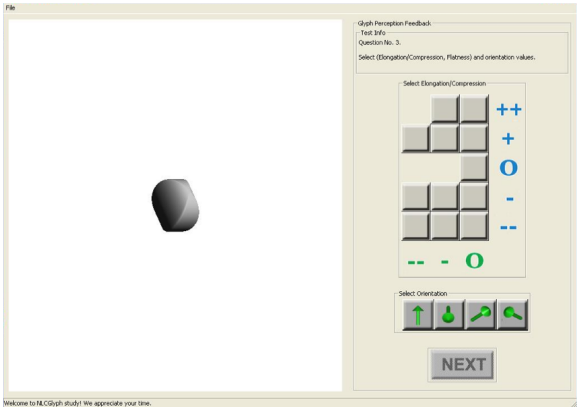

Figure 3: *Screen shot of the user interface.*

ally symmetric and strongly suggest orientation along the long axis of the shape. Ellipsoidal glyphs, described first for NLC physics by Allen [All89] and used subsequently elsewhere [FWZ01, SPL*06], can vary their different symmetries by changing the ratio of the major, medium, and minor axes. Finally, superellipsoids [JKM06] not only change their symmetry, but their underlying shape; the superellipsoid shape parameters vary between box-, sphere-, and cylinder-like appearance depending upon the NLC tensor. While the perceptual saliency of superquadrics have been studied in general visualization [ERS*00], we have found no work that has previously studied the effectiveness of the four major NLC tensor glyphs. That is the purpose of our study.

3. First Tensor Glyph Experiment

To evaluate the different real symmetric traceless tensor glyphs, we designed an experimental framework to measure a user's comprehension of the three properties communicated by the glyphs: Orientation, uniaxiality, and biaxiality. We had several goals for our study:

- Under orientation, glyphs representing different tensor values may appear the same due to lighting (ellipsoids are known for this behavior [Kin04]). We wished to find out how orientation affects the perceived values of the other glyphs parameters.
- The four glyphs highlight different aspects of the system. We wanted to discover if the more versatile glyphs (ellipsoid and superellipsoid) would communicate the tensor parameters more accurately.
- Though shape perception is rapid in the visual system, the conjunctive properties of glyphs (orientation, shape, lengths, etc.) make their comprehension more difficult [War04]. Thus, we measured response time in order to determine the difficulty in understanding each glyph.

In NLC tensor visualizations, glyphs are not displayed alone; a volume is populated with glyphs to communicate the spatial behavior of the NLC substrate. Such a study is beyond the scope of this effort. Our focus is on understanding how single glyphs are comprehended; further work on the larger scope is an eventual goal.

3.1. Experimental Task

Our experimental framework includes a user interface for testing (Figure 3). For each trial, a single glyph was presented to the user. The user was then prompted to click on the button which identified the glyph's orientation and then click on the button corresponding to the glyph's combined uniaxial and biaxial properties; users were free to select the uniaxial/biaxial properties before orientation if desired and were allowed to change their selection. Once a final selection of properties was made, the user clicked the "Next" button to record their choices and response time, and view another glyph. This process was repeated until all combinations of glyphs were seen.

Table 2: *Independent and Dependent Variables*

INDEPENDENT VARIABLES		
subject	17	(random variable)
glyph	5	box cylinder ellipsoid super-e (superellipsoid) (not reported)
orientation	4	F-N (far to near) B-T (bottom to top) LBF-RTN (left-bottom-far to right-top-near) RBF-LTN (right-bottom-far to left-top-near)
uniaxiality	5	$--, -, 0, +, ++$
biaxiality	3	$--, -, 0$
DEPENDENT VARIABLES		
orientation error	0 if correct orientation 1 if incorrect orientation	
uniaxial error	*measured uniaxiality* $-$ *uniaxiality*	
biaxial error	*measured biaxiality* $-$ *biaxiality*	
total error	$\frac{1}{3}$ (*orientation err.* $+ \lvert$*uniaxial err.*$\rvert /$(*max uni. err.*) $+ \lvert$*biaxial err.*$\rvert /$(*max biaxial err.*))	
response time	seconds	

All subjects viewed glyphs on the same LCD monitor in the same lab space; a laptop connected to an external mouse was used as the experimental machine. Directional lighting for the glyphs came from $\mathbf{l} = [3,2,4]$ in eye coordinates (just off one of the main diagonals), and all glyphs were rendered using the same number of polygons. The software was written in C++ using OpenGL and wxWidgets.

3.2. Variables and Design

3.2.1. Independent variables

Table 2 enumerates the experimental variables used in our glyph study. Our four independent variables sample the space of possible tensors over the tested glyph types. A roughly uniform sampling was used to cover the glyph space while limiting the total number to minimize subject fatigue during the experiment. These variables are described next.

Subjects Seventeen subjects were recruited from a population of undergraduate and graduate students varying in age from 19–28; most were electrical/computer engineers or computer scientists, with additional students from Business Information Systems and Industrial Engineering. One participant was female. Each participant was given a spatial ability test based on other's tests [Det, TFU04] as a screening method; all subjects but one scored at least 75%, with an mean of $89\% \pm 11\%$. Subjects were unpaid volunteers.

Glyph Type In our first experiment, five glyph types were presented to the user. Four of them correspond to the shapes previously mentioned: Boxes [SKH95], cylinders [AWB01], ellipsoids [All89, FWZ01, SPL*06], and superquadric ("super-e") [JKM06]. A fifth glyph, a modified ellipsoid, was determined after testing to be an incorrect implementation of a previous method that was covered by our extant ellipsoidal glyph. Since the fifth glyph type did not properly encode the tensor parameters (it was always rotational symmetric, failing to encode biaxiality), its results were discarded and are not reported.

Orientation Canonically, our glyphs are aligned with $\hat{\mathbf{x}}$ before rotation; the orientation variable determines this rotation. Four orientations were used: Bottom-to-top ("B-T") along $+\hat{\mathbf{y}}$ in the eye-coordinate frame, far-to-near ("F-N") along $+\hat{\mathbf{z}}$, left-bottom-far to right-top-near ("LBF-RTN") along $\mathbf{v}_{\text{LBF-RTN}} = [1,1,1]$, and right-bottom-far to left-top-near ("RBF-LTN") along $\mathbf{v}_{\text{RBF-LTN}} = [-1,1,1]$. Since the director is headless (vector sign is irrelevant), these directions cover four out of seven major directions on a hemi-cube (towards its faces or corners). Two directions are on-axis to minimize depth effects; one of the off-axis orientations is nearly parallel with the scene's light to evaluate shading. Adding additional orientations, while providing an more in-depth look at the space, would unreasonably increase the experimentation time to over two hours based upon our test results; the orientations chosen exhibit the most differences.

It is important to note that in the isotropic case (when $\mathbf{Q} = \mathbf{0}$ and $S = 0$), orientation is undefined. Thus, though a canonical orientation was provided to the experimental framework, all orientations were accepted as valid user-selected values.

Uniaxiality The strength of uniaxial alignment determines the amount by which the molecules align along the director (positive) or in the plane orthogonal to the director (negative) [MN04, Muk98]. When aligned with the director, the shape is elongated along that orientation like a rod; when aligned with the plane orthogonal, the shape is compressed with respect to the orientation like a disc. In between, in the isotropic case, there is no alignment, and the shape is essentially a sphere or other regular shape. We used this intuitive metaphor—elongation along or compression against the orientation—to describe the uniaxiality property to users; the term uniaxial was never used.

For the experiment, five levels of uniaxial strength (or elongation/compression) where used: Maximally compressed ("$--$" at $S = -\frac{1}{2}$), somewhat compressed ("$-$" at $S = -\frac{1}{4}$), neither compressed or elongated ("0" at $S = 0$), somewhat elongated ("$+$" at $S = \frac{1}{2}$) and maximally elongated ("$++$" at $S = 1$).

Biaxiality In a pure uniaxial configuration, nematic molecules are rotationally symmetric. As biaxiality increases, the collection of molecules exhibit increasing reflective symmetry. This process is akin to flattening a tensor shape parallel to the director to introduce the reflective symmetry. As in the uniaxial case, we used the intuitive concept

of "flattening" to describe biaxiality. Three levels of biaxiality/flattening were used in the study: No flattening ("0" at $b = 0$), some flattening ("−" at $b = \frac{1}{2} b_{\max}$), and maximum flattening ("−−" at $b = b_{\max}$) where $b_{\max} = \frac{1}{3} |S|$ is the relative maximum biaxiality for a given uniaxial arrangement. In cases where the level of biaxiality was invalid (such for any non-zero b when $S = 0$), users were not allowed to provide that option (no button for the S/b combination existed in the user interface (Figure 3)). For all glyphs, the axis of biaxiality $\mathbf{m}$—the axis with the larger absolute eigenvalue—was always $\hat{\mathbf{y}}$ in the glyph's local frame (i.e., before rotation).

3.2.2. Dependent variables

Two sets of dependent variables were gathered: Error metrics for each tensor property and the user's response time.

Error Metrics For each major tensor property (orientation, uniaxiality, and biaxiality), an error metric is defined. Orientation errors are binary: Either the user selected the correct orientation or an error occurred; no gradation between orientations is used. Finer distinctions are used for uniaxial and biaxial error: The error is the signed distance from the user's selection and the correct selection. Given the range of uniaxial selections (-2 to 2) and biaxial selections (-2 to 0), the possible error values are between -4 and 4 for uniaxial error and -2 to 2 for biaxial error respectively. This distance is not based upon the tensor values (S or b) but on the user perceived values (e.g., −− or +). This distinction facilitates data analysis and better matches the user's model of the problem as they were not privy to the internal workings of the tensor representation.

To represent total error, the sum of errors was normalized; the absolute value of the normalized uniaxial and biaxial errors were used to ignore sign. This error terms gives equal weight to each of the three errors.

Response Time The time for a subject to select the glyph properties and move to the next glyph was recorded; all times are measured in seconds. No timeout was used; subjects could take as much time as they wanted.

3.2.3. Experimental Procedure

A $5 \times 4 \times 5 \times 3$ factorial nesting of the independent variables from Table 2 was used to gather data. To account for learning and fatigue effects, we counterbalanced presentation order using a 5×5 Latin square for the primary variable (glyph) and random permutations for the other variables. The study was a within-subjects design; each user saw all valid combinations of variables. 4080 data points were gathered (12 combinations of uniaxiality and biaxiality per orientation $\times$ 4 orientations $\times$ 5 glyphs types (including the unreported glyph) $\times$ 17 users). With the invalid glyph removed, 3264 data points were analyzed.

For each subject, the study progressed through several stages. First, the users signed a consent form and took the spatial ability test previously mentioned. The users were then given a set of cards representing each glyph type (a larger reproduction of Figure 2, one card for each glyph type) and the three parameters (orientation, elongation/compression, and flatness) were described. The users were then shown a common set of 10 glyphs as part of a practice period. Afterwards, the subjects completed 5 blocks of 48 trials—one repetition of every combination of glyph parameters. Since fully learning each glyph would likely take longer than the allotted testing period, subjects were allowed to keep the reference cards. After the trials, subjects were asked a follow-up questionnaire to evaluate the design of the study. All together, the subjects took 90 to 120 minutes to complete the entire experimental procedure.

4. First Experiment Results

For the 17 subjects, a total of 3264 trials were completed, each providing four error metrics and a response time. We analyzed the data using error plots, a χ^2 test for orientation error, and balanced analysis of variance (ANOVA) for the other measures. When using ANOVA, our experiment was modeled as a repeated-measures design using subject as a random factor and the other independent variables as fixed. Since our experiment is a within-subjects design, ANOVA's assumptions about the normal distribution of measures and homogeneity of variance could be violated. Thus, as per Howell (p. 486) [How02], we applied the Huynh-Feldt correction ε to each F-test by modifying the test's degrees of freedom by ε; this results in a more conservative test that corrects for lack of sphericity (validity of ANOVA's assumptions). At no time during our analysis did the Huynh-Feldt correction change the results of an F-test from significant to non-significant. Table 3 tabulates the ANOVA tests.

Before analysis, we processed outliers for the response time data using the method of Barnett and Lewis [BL94]. Histograms for each dependent measure were examined. A bimodal distribution was observed for orientation error, a multimodal distribution for total error, a skewed normal distribution for response time, and a symmetric normal distributions for uniaxial and biaxial error. Large numbers of outliers (found in the distribution's tails after gaps) were only found in the response time data; each was replaced by the median of the other values sharing the same subject, glyph, and orientation. As outliers are treated as mistaken values, this method improves the calculations of statistics relevant to the ANOVA (means, standard errors, and sum-of-squares), which would otherwise be adversely affected by the outlying terms. As a final part of preparing the analysis, we tested for learning and fatigue effects; we did not find evidence of either within the results and thus do not address them.

4.1. Glyphs and Orientation

We first analyzed the effect of glyph on orientation errors. The orientation of a glyph provides a frame of reference

	Dependent Variable	Effect	$F(df, df)$	p	ϵ
(a)	Orientation Error	**Main Effect of Glyph**	$F(2.0, 31.9) = 43.7$	$p < 0.001$	$\epsilon = 0.644$
(b)	Orientation Error	**Main Effect of Orientation**	$F(3.0, 47.7) = 12.8$	$p < 0.001$	$\epsilon = 0.995$
(c)	Orientation Error	**Glyph by Orientation Interaction**	$F(4.1, 65.2) = 23.6$	$p < 0.001$	$\epsilon = 0.453$
(d)	Uniaxial Error	Main Effect of Glyph	$F(3.0, 48.0) = 1.1$	$p = 0.369$	$\epsilon = 1.0$
(e)	Uniaxial Error	**Main Effect of Orientation**	$F(2.4, 38.2) = 17.2$	$p < 0.001$	$\epsilon = 0.795$
(f)	Uniaxial Error	**Glyph by Orientation Interaction**	$F(5.5, 87.6) = 6.8$	$p < 0.001$	$\epsilon = 0.608$
(g)	Biaxial Error	Main Effect of Glyph	$F(2.4, 38.9) = 0.126$	$p = 0.915$	$\epsilon = 0.810$
(h)	Biaxial Error	**Main Effect of Orientation**	$F(2.9, 45.7) = 19.8$	$p < 0.001$	$\epsilon = 0.951$
(i)	Biaxial Error	**Glyph by Orientation Interaction**	$F(6.3, 100.2) = 3.9$	$p < 0.001$	$\epsilon = 0.696$
(j)	Total Error	**Main Effect of Glyph**	$F(2.1, 32.7) = 22.4$	$p < 0.001$	$\epsilon = 0.682$
(k)	Total Error	**Main Effect of Orientation**	$F(2.0, 32.5) = 13.5$	$p < 0.001$	$\epsilon = 0.677$
(l)	Total Error	**Glyph by Orientation Interaction**	$F(6.0, 95.7) = 35.0$	$p < 0.001$	$\epsilon = 0.664$
(m)	Response Time	Main Effect of Glyph	$F(2.4, 38.4) = 1.14$	$p = 0.264$	$\epsilon = 0.799$
(n)	Response Time	Main Effect of Orientation	$F(2.4, 38.9) = 1.5$	$p = 0.239$	$\epsilon = 0.809$
(o)	Response Time	**Glyph by Orientation Interaction**	$F(6.9, 110.7) = 3.470$	$p < 0.001$	$\epsilon = 0.769$

Table 3: *ANOVA results for the first experiment with corrections due to non-sphericity. Significant effects are highlighted.*

for the other parameters: The direction along which uniaxial alignment occurs and the plane in which biaxiality occurs. As such, properly communicating orientation is vital for tensor glyphs.

To analyze orientation errors due to glyph type, we first examined the frequency of orientation error for each glyph type. Of our 3264 data points, only 126 (3.9%) had orientation errors, and we did find an effect of glyph type among these errors ($\chi^2(3) = 159.0$, $p < 0.001$). Superellipsoids (1 orientation error) and cylinders (6 errors) fared much better than ellipsoid (29 errors) and box glyphs (90 errors). As anticipated, ellipsoids exhibit more errors due to rotation than the superellipsoids and cylinders which both use shape to indicate the direction of alignment. What is surprising, however, is that boxes perform so poorly —the box glyph also indicates the director's direction using shape. To explain this finding requires further analysis.

We next investigated the interaction between glyph and orientation on orientation error (Figure 4). We found a main effect of glyph (Table 3a) and a main effect of orientation (Table 3b); both effects are explained by a glyph by orientation interaction (Table 3c). This interaction clarifies the source of orientation error for box glyphs: Errors predominate for on-axis alignments (B-T and F-N). In this configurations, no lighting cues are present—the box surface is flat shaded. It is thus likely that the B-T and F-N orientations are being confused. When strong lighting cues are present (off-axis orientations), the mean error rate falls dramatically.

As for ellipsoids, unlike the other glyphs, their mean error increases with off-axis alignments (Figure 4, LBF-RTN and RBF-LTN orientations). If we study the non-box glyphs, the main effect of orientation and the glyph by orientation are eliminated, leaving the main effect of glyph only ($F(1.1, 17.3) = 5.45, p = 0.03, \varepsilon = 0.541$). This suggest there is a difference amongst the three remaining glyph types, although post-hoc comparison of the means did not find individual differences. Overall, the cylinder and superellipsoid glyphs accurately communicate the director regardless of orientation.

4.2. Glyphs and Other Errors

We used ANOVA to compare the remaining glyph error metrics. For uniaxial error, there was no main effect of glyph (Table 3d), but there was a main effect for orientation (Table 3e) and a glyph by orientation interaction (Table 3f). Figure 5 depicts the interaction between glyph type and orientation for uniaxial error. Subjects tended to underestimate uniaxiality for non-canonical orientations (ones not B-T, differences are significant from post-hoc analysis with $p < 0.025$). The non-box glyphs followed roughly the same trend for uniaxiality; their differences are still significant and the interaction is removed if the box glyph is excluded from the analysis ($F(2.7, 43.8) = 4.7, p = 0.007, \varepsilon = 0.913$). Examining the graph, box glyphs again performed poorly for the on-axis alignments, especially in the F-N case. For the box

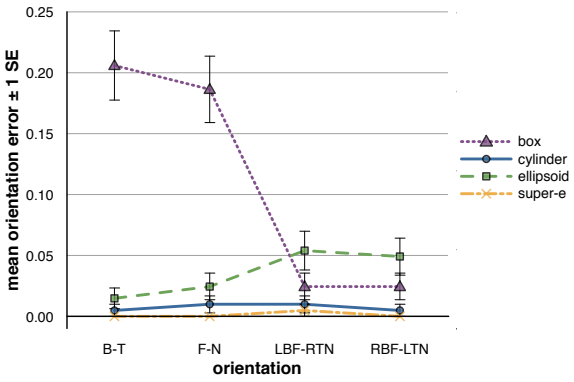

Figure 4: *Orientation vs. mean orientation error by glyph type. Error bars for all charts are one standard error.*

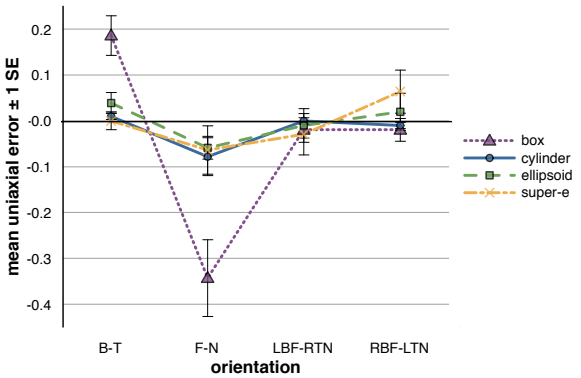

Figure 5: *Orientation vs. mean uniaxial error by glyph type.*

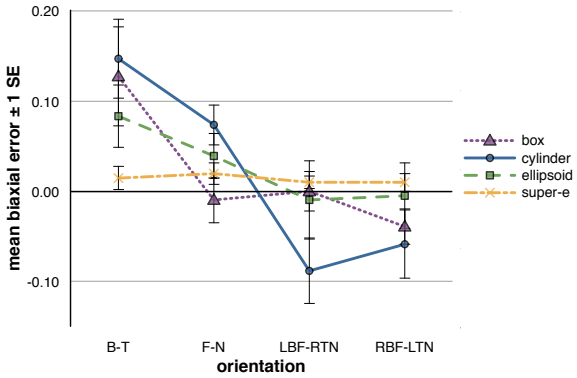

Figure 6: *Orientation vs. mean biaxial error by glyph type.*

glyphs, uniaxiality is encoded along the director, and because the director is parallel to the viewer in the F-N orientation, uniaxiality is visually lost in this case.

For biaxial error, there was no main effect of glyph (Table 3g), but there was a main effect of orientation (Table 3h) and a glyph by orientation interaction (Table 3i). Figure 6 depicts the interaction between glyph type and orientation for biaxial error. Here users tended to underestimate for axis-aligned configurations (negative values indicate more biaxiality in the figure); individual differences between the B-T configuration and all others and F-N and the off-axis configurations were significant in post-hoc analysis ($p < 0.002$). Biaxiality errors were overall smaller in the off-axis orientations. All the glyphs use the relative difference of widths along the medium and minor eigenvectors to encode biaxiality; only superellipsoids also use shape to visually encode this parameter. Since this relative difference cannot be seen in the B-T case, subjects had a harder time identifying the biaxiality for non-superellipsoids. For the other orientations, the relative difference can be seen, explaining the decrease in error. Unlike the other glyphs, superellipsoids maintained a constant level of error for all orientations, a slight overestimation.

Total error (Figure 7) exhibits effects that combine its three components. Analysis shows that total error has a main effect of glyph and orientation with a glyph by orientation interaction (Table 3k–l). The trends of the box and ellipsoid errors follow that of their orientation error (Figure 4), indicating that orientation error dominates for these glyphs. The profile for cylinder and superellipsoid glyphs are roughly flat; however, cylinder glyphs have more total error overall, most likely from the influence of its biaxial errors (Figure 6). Post-hoc analysis of the difference between the means shows the superellipsoid's error is significantly lower than the other glyphs; significant differences are also found between cylinders and boxes overall (Table 4).

	Mean	SD	*p*-value for Difference Box	Cyl.	Ell.	Sup.
Box	0.090	0.17	—	< 0.000	0.073	< 0.000
Cyl.	0.047	0.09	< 0.000	—	1.000	< 0.000
Ell.	0.058	0.12	0.073	1.000	—	0.023
Sup.	0.016	0.06	< 0.000	< 0.000	0.023	—

Table 4: *Descriptive statistics and post-hoc significance of marginal means for total error; significant differences highlighted ($\alpha = 0.05$). Adjustments for multiple comparison made using the Bonferroni correction.*

4.3. Glyphs and Response Time

Subjects' response time exhibited complex behavior. No main effect due to glyph or orientation was observed (Table 3m,n); however, there was an interaction between the two (Table 3o). We did not see this interaction again in the follow-up experiment, nor were the differences between the means significant, so there is little conclusive that may be said about the response time differences.

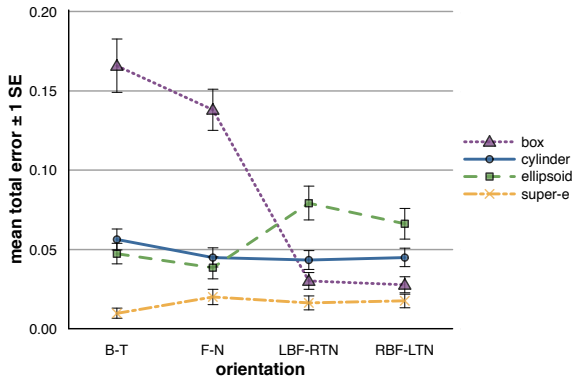

Figure 7: *Orientation vs. mean total error by glyph type.*

	Dependent Variable	Effect	$F\,(df, df)$	p	ϵ
(a)	Orientation Error	**Main Effect of Glyph**	$F\,(2.5, 29.5) = 31.0$	$p < 0.001$	$\epsilon = 0.819$
(b)	Orientation Error	**Main Effect of Orientation**	$F\,(1.8, 22.1) = 7.2$	$p = 0.005$	$\epsilon = 0.615$
(c)	Orientation Error	**Glyph by Orientation Interaction**	$F\,(4.2, 49.8) = 16.1$	$p < 0.001$	$\epsilon = 0.461$
(d)	Uniaxial Error	**Main Effect of Glyph**	$F\,(1.8, 21.6) = 3.6$	$p = 0.049$	$\epsilon = 0.600$
(e)	Uniaxial Error	**Main Effect of Orientation**	$F\,(1.9, 22.8) = 4.6$	$p = 0.029$	$\epsilon = 0.634$
(f)	Uniaxial Error	**Glyph by Orientation Interaction**	$F\,(7.0, 84.0) = 6.2$	$p < 0.001$	$\epsilon = 0.778$
(h)	Biaxial Error	**Main Effect of Orientation**	$F\,(2.1, 25.7) = 7.9$	$p = 0.002$	$\epsilon = 0.715$
(i)	Biaxial Error	**Glyph by Orientation Interaction**	$F\,(7.8, 93.5) = 2.3$	$p = 0.027$	$\epsilon = 0.865$
(j)	Total Error	**Main Effect of Glyph**	$F\,(3.0, 36.0) = 34.1$	$p < 0.001$	$\epsilon = 1.0$
(k)	Total Error	**Main Effect of Orientation**	$F\,(3.0, 35.8) = 13.0$	$p < 0.001$	$\epsilon = 0.996$
(l)	Total Error	**Glyph by Orientation Interaction**	$F\,(7.5, 90.0) = 24.1$	$p < 0.001$	$\epsilon = 0.834$

Table 5: *Significant ANOVA results for the second experiment with corrections due to non-sphericity. Compare Table 3.*

5. Second Experiment

Though our first experiment showed strong statistical results, we wanted to ensure that the additional time taken by subjects to process the fifth, unreported glyph type did not affect their overall behavior significantly. To this end, we ran a second iteration of the experiment identical to the first with the erroneous glyph type removed; we used a 4×4 balanced Latin square to counterbalance glyph presentation order, and all other aspects of the design were the same. Eleven male and two female subjects between the ages of 23–34 were tested from a similar population as before; no subject took the experiment both times. For the 13 subjects, 2496 trials were completed; we performed a similar analysis as before on this data. The significant results of the ANOVA tests are found in Table 5.

Overall, the results of the second study followed those of the first. As before, only 3% (81 out of 2496) of the trials had orientations errors; the different number of errors (55 box, 4 cylinder, 18 ellipsoid, 4 superellipsoid) were significant ($\chi^2\,(3) = 86.0, p < 0.001$), with boxes dominating. All previously significant results in the first experiment were significant in the second experiment save for response time which showed no significant interaction ($F\,(8.0, 96.4) = 50.5$, $p = 0.175$, $\varepsilon = 0.892$); a new (weak) interaction of glyph and orientation for uniaxial error was also observed (Table 5d). There were significant post-hoc differences between the box glyph and the other glyphs for orientation error ($p < 0.001$ at the highest) as it continued to fair poorly for axis-aligned configuration. Biaxial error followed a similar trend as in the first experiment with significant post-hoc differences between the F-N and off-axis configurations ($p < 0.008$); trends for the total error were essentially identical as before with superellipsoids performing significantly better than the others in post-hoc analysis ($p < 0.002$). As for response time, the loss of significant effect is possibly due to the larger standard error and lower power compared to the first experiment; more subjects would be needed to resolve this effect. The behavior of the response time was largely different, although again superellipsoids provided the lowest overall response time. Excluding response time, the second study replicated the results of the first, indicating that the results reported here are reliable despite the presence of the extraneous-glyph.

6. Discussion

Of the four glyph types studied, superquadric glyphs performed consistently better than the other glyphs, with lower total error and generally lower response time over all orientations. Cylinders had low total error, though they exhibited more significant biaxiality errors than the superquadric glyphs. With clear lighting (on-axis arrangements), ellipsoids faired quite well, with similar response times and total error as cylinders. However, off-axis arrangements introduce shading artifacts that seem to confound perception of the tensor properties and take longer to process. Finally, box glyphs did poorly in the on-axis arrangements, especially with respect to uniaxiality. But, in contrast to ellipsoids, boxes exhibited relatively low error on the off-axis arrangements, suggesting that lighting cues are more important to distinguish tensor properties for the faceted shape. Figure 8 summarizes the performance findings of our study.

Each of the four glyphs use different strategies to communicate the tensor parameters. The superquadric glyphs dually encode each parameter: Orientation via the glyph's alignment and the apex of the shape, uniaxiality via the shape and height of the glyph, and biaxiality via the shape and the relative width/depth of the glyph. The distinct change in the glyph's shape likely reduced the subjects' error in identify the shape mentally or on the reference sheet. The strong alignment cue of the cylinder glyph (its axis of rotation) kept orientation error low; however, this same rotational symmetry seems to have interfered with perception of biaxiality. As mentioned, ellipsoids faired poorly due to ambiguity; however, they did communicate biaxiality reasonably well. Finally, the reflective symmetry of the box did assist in conveying biaxiality (for orientations other than B-T), but the shape had little other advantage.

Though the glyphs studied are specifically for nematic liquid crystal visualization, some lessons extend to wider tensor

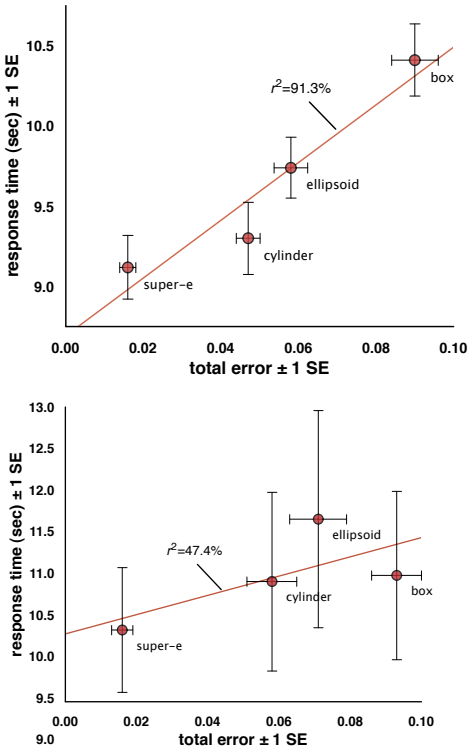

Figure 8: *Plot of total error vs. response time with linear fit, first experiment (top) and second experiment (bottom).*

depiction. All of our findings are directly applicable to general real symmetric traceless tensor visualization as the three major properties of NLC glyphs—orientation, the size of the major eigenvalue (uniaxiality) and amount of divergence of the medium and minor eigenvalues (biaxiality)—have direct analogs for general tensors. Our observation about the visual ambiguity of ellipsoid glyphs validates the design motivation of Kindlmann for his superquadric DT-MRI glyphs [Kin04]; however, the specific design of his glyphs has not been tested. Similarly, our findings with regard to glyph type and orientation are suggestive for non-superellipsoid glyphs, regardless of application. Our results imply that dual encoding of tensor parameters is beneficial, and should be factored into future tensor glyph designs.

While this study answers several questions about tensor glyphs, there are some caveats. Our work measures glyph perception in isolation; it does not address the issue of larger groups of glyphs. Though it is likely there are correlations between the two settings, additional studies are needed to fully address this issue. Secondly, this study does not address learnability or expertise with regard to the glyphs; subjects' exposure to the glyphs were too short and follow-up studies were not performed. Finally, encoding of tensor properties with means other than shape were not studied. Textures and colors have important roles in perception, and the guidance of previous work [BHW06, HE99, HBW06, KHSI04, UIL*06] could be used for follow-up studies.

7. Conclusions and Future Work

We have presented a study evaluating the effectiveness of four tensor glyphs for nematic liquid crystal visualization. Superquadrics glyphs performed best overall while box glyphs performed the poorest; cylinders and ellipsoids fell between. The redundant encoding of the superquadrics appears to address the visual ambiguity present in ellipsoidal and box glyphs while correcting for the biaxiality issues of the cylinder approach. Our findings also provide guidance to other tensor glyphs.

Besides follow-up studies on collections of glyphs and glyphs for other visualization domains, there is possible additional future work. Glyphs are not the only method to visualize NLC tensors; streamtubes and streamlines have also been used [SPL*06]. As these shapes must also communicate the tensor properties, a similar study could be conducted to analyze their perceptual effectiveness.

Acknowledgments

We thank Ketan Mehta for his initial work on this project and Gordon Kindlmann, Vladim Slavin, Andrew Callan-Jones, David Laidlaw, and Robert Pelcovits for valuable discussions. This work was partially funded through the National Science Foundation EPSCoR program via award #0132618.

References

[All89] ALLEN M. P.: Molecular graphics and the computer simulation of liquid crystals. *Molecular Simulation 2*, 4 (February 1989), 301–306.

[AWB01] ANDERSON J. E., WATSON P., BOS P. J.: Comparisons of the vector method and tensor method for simulating liquid crystal devices. *Liquid Crystals 28* (2001), 109–115.

[Bar81] BARR A. H.: Superquadrics and angle-preserving transformations. *IEEE Computer Graphics and Applications 1*, 1 (April 1981), 11–22.

[BH04] BENGER W., HEGE H.-C.: Tensor splats. In *Visualization and Data Analysis 2004, Proc. of SPIE* (June 2004), vol. 5295, pp. 151–162.

[BHW06] BAIR A., HOUSE D. H., WARE C.: Texturing of layered surfaces for optimal viewing. *IEEE Transactions on Visualization and Computer Graphics (Proceedings Visualization/Information Visualization 2006) 12*, 5 (2006), 1125–1132.

[BL94] BARNETT V., LEWIS T.: *Outliers in Statistical Data*, 3rd ed. John Wiley and Sons, 1994.

[Col02] COLLINGS P. J.: *Liquid Crystals: Nature's Delicate Phase of Matter*, 2nd. ed. Priceton University Press, Princeton, NJ, 2002.

[Det] DETTERMAN D. K.: Intelligence. in Microsoft Encarta Online. http://encarta.msn.com/encyclopedia_761570026/Intelligence.html (Checked March 2008).

[dG74] DE GENNES P. G.: *The Physics of Liquid Crystals*. Clarendon, Oxford, 1974.

[ERS*00] EBERT D. S., ROHRER R. M., SHAW C. D., PANDA P., KUKLA J. M., ROBERTS D. A.: Procedural shape generation for multi-dimensional data visualization. *Computers & Graphics 24*, 3 (2000), 375–384.

[FWZ01] FOREST M. G., WANG Q., ZHOU H.: Methods for the exact construction of mesoscale spatial structures in liquid crystal polymers. *Physica D 152–153* (2001), 288–309.

[HBW06] HOUSE D. H., BAIR A., WARE C.: An approach to the perceptual optimization of complex visualizations. *IEEE Transactions on Visualization and Computer Graphics 12*, 4 (2006), 509–521.

[HE99] HEALEY C. G., ENNS J. T.: Large datasets at a glance: Combining textures and colors in scientific visualization. *IEEE Transactions on Visualization and Computer Graphics 5*, 2 (Apr. 1999).

[How02] HOWELL D. C.: *Statistical Methods for Psychology*, 5th ed. Duxbury, Pacific Grove, CA, 2002.

[JKM06] JANKUN-KELLY T. J., MEHTA K.: Superellipsoid-based, real symmetric traceless tensor glyphs motivated by nematic liquid crystal alignment visualization. *IEEE Transactions on Visualization and Computer Graphics (Proceedings Visualization/Information Visualization 2006) 12*, 5 (September/October 2006), 1197–1204.

[KHSI04] KIM S., HAGH-SHENAS H., INTERRANTE V.: Conveying shape with texture: Experimental investigations of texture's effects on shape categorization judgments. *IEEE Transactions on Visualization and Computer Graphics 10*, 4 (July/Aug. 2004), 471–483.

[Kin04] KINDLMANN G. L.: Superquadric tensor glyphs. In *Proceedings of the Eurographics/IEEE VGTC Symposium on Visualization (VisSym '04)* (2004), Deussen O., Hansen C., Keim D. A., Saupe D., (Eds.), pp. 147–154.

[KW99] KINDLMANN G., WEINSTEIN D.: Hue-balls and lit-tensors for direct volume rendering of diffusion tensor fields. In *VISUALIZATION '99: Proceedings of the 10th IEEE Visualization 1999 Conference (VIS '99)* (Washington, DC, USA, 1999), IEEE Computer Society.

[KWH00] KINDLMANN G., WEINSTEIN D., HART D.: Strategies for direct volume rendering of diffusion tensor fields. *IEEE Transactions on Visualization and Computer Graphics 6*, 2 (2000), 124–138.

[MN04] MORRTRAM N., NEWTON C.: *Introduction to Q-tensor theory*. Tech. rep., Dept. of Mathematics, University of Strathclyde, 2004.

[Muk98] MUKHERJEE P. K.: Critical behavior of uniaxial–biaxial nematic phase transition. *The Journal of Chemical Physics 109*, 7 (1998), 2941–2946.

[SEHW02] SIGFRIDSSON A., EBBERS T., HEIBERG E., WIGSTRÖM L.: Tensor field visualisation using adaptive filtering of noise fields combined with glyph rendering. In *VIS '02: Proceedings of the conference on Visualization '02* (Washington, DC, USA, 2002), IEEE Computer Society, pp. 371–378.

[SEK*98] SHAW C. D., EBERT D. S., KUKLA J. M., ZWA A., SOBOROFF I., ROBERTS D. A.: Data visualization using automatic, perceptually-motivated shapes. In *Proceedings of Visual Data Exploration and Analysis* (Apr. 11 1998), SPIE.

[SKH95] SONNET A., KILIAN A., HESS S.: Alignment tensor versus director: Description of defects in nematic liquid crystals. *Physical Review E 52* (July 1995), 718–722.

[SPL*06] SLAVIN V. A., PELCOVITS R. A., LORIOT G., CALLAN-JONES A., LAIDLAW D. H.: Techniques for the visualization of topological defect behavior in nematic liquid crystals. *IEEE Transactions on Visualization and Computer Graphics (Proceedings Visualization/Information Visualization 2006) 12*, 5 (September/October 2006), 1323–1328.

[TFU04] TOMAI E., FORBUS K. D., USHER J.: Qualitative spatial reasoning for geometric analogies. In *Proceedings of the 18th International Qualitative Reasoning Workshop* (2004).

[UIL*06] URNESS T., INTERRANTE V., LONGMIRE E., MARUSIC I., O'NEILL S., JONES T. W.: Strategies for the visualization of multiple 2D vector fields. *IEEE Computer Graphics and Applications 26*, 4 (2006), 74–82.

[War04] WARE C.: *Information Visualization: Perception for Design*, second ed. Morgan Kaufmann Publishers, 2004.

[ZLK04] ZHANG S., LAIDLAW D. H., KINDLMANN G. L.: Diffusion tensor MRI visualization. In *The Visualization Handbook*, Hansen C. D., Johnson C. R., (Eds.). Elsevier Academic Press, 2004, ch. 16, pp. 327–340.